Journal of Applied Mechanics and Technical Physics, Vol. 41, No. 1, 2000

APPEARANCE OF A "COLD" LAYER UPON EXPLOSIVE COMPACTING OF POWDERS

A. E. Buzyurkin and S. P. Kiselev

UDC 539.374

Explosive compacting of powders is numerically simulated in the two-dimensional formulation. Different flow regimes depending on the detonation velocity are considered. Based on the calculations, the nature of the appearance of a "cold" layer upon explosive compacting of powders is revealed.

Upon compacting of powder materials under conditions of two-dimensional explosive loading, zones of structural inhomogeneities located near the interface between the powder and deformed target can appear. In particular, low-temperature "cold" zones were observed in plane or cylindrical powder compacts containing a monolithic rod (centerbody), which is a flat plate in the two-dimensional case. In these zones, the compacting process was not accompanied by a significant increase in temperature [1]. The "cold" layer is understood as a layer in which the particles are not "welded" and experience a significantly lower local deformation than the particles in the outer layer. The nature of formation of these zones has not been clarified yet. According to Kostyukov [2], the "cold" layer appears if the following inequality is satisfied:

$$D < D_*,$$

Here D is the velocity of propagation of a detonation wave and $D_* \approx C_0$ is the velocity of propagation of a shock wave in a plate, which is close to the volume speed of sound C_0 under given loads. The shock-wave pattern arising in this case was qualitatively analyzed by Kiselev and Fomin [3] and is shown in Fig. 1.
A hillock BC arises on the plate surface MLKN ahead of the shock-wave front AOC. This hillock generated a weak shock wave OB. In the inner layer LGFK, the powder LHIK is compressed in shock waves OB, OC, and EC. It is assumed that the powder is compressed to dense packing in the weak shock wave OB; therefore, the irreversible losses of thermal energy related to plastic collapsing of the pores (particle-shape variation) are small, and the particles are not "welded." It is the continuous material that is compressed in the shock wave OC; hence, the thermal energy changes weakly, and the internal energy is changed due to increasing energy of cold compression. In the outer layer GHIF, significant thermal energy is released upon plastic collapsing of the pores in a strong shock wave emanating from the explosive (Ω is the region occupied by explosion products and ASRI is the nonreacted explosive), which leads to "welding" of the particles with each other (Fig. 1).

It should be noted that the previous two-dimensional numerical calculations [1] did not register the formation of a hillock on the centerbody surface ahead of the shock wave in the powder for $D < C_0$. The reason is not clear because Kusubov et al. [1] did not give the equation of state of the powder used in the calculations. The dynamic experiments of Kostyukov [4] revealed only an indirect effect of the hillock on density variation, and the hillock itself was obtained only at one point corresponding to conditions $D = C_0$. All this makes actual numerical simulation of this problem difficult.

Institute of Theoretical and Applied Mechanics, Siberian Division, Russian Academy of Sciences, 630090 Novosibirsk. Translated from Prikladnaya Mekhanika i Tekhnicheskaya Fizika, Vol. 41, No. 1, pp. 192–197, January–February, 2000. Original article submitted January 28, 1999.

 0021-8944/00/4101-0176 $25.00 © 2000 Kluwer Academic/Plenum Publishers

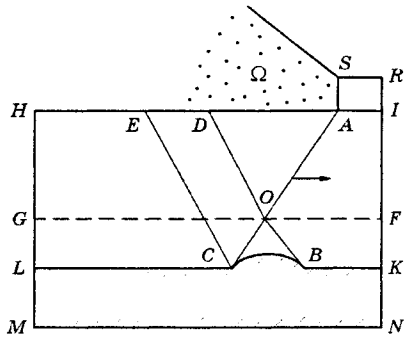

Fig. 1

Equations that describe the behavior of a porous elastoplastic medium are based on the laws of conservation of mass, momentum, and energy and have the form [5, 6]

$$\frac{\partial \rho}{\partial t} + \nabla_i \rho v_i = 0, \qquad \rho = \rho_s m_2, \qquad m_1 + m_2 = 1,$$

$$\rho \frac{dv_i}{dt} = \nabla_j \sigma_{ij}, \qquad \frac{d}{dt} = \frac{\partial}{\partial t} + v_i \nabla_i, \qquad \nabla_i = \frac{\partial}{\partial x_i},$$

$$\rho \frac{dE}{dt} = \sigma_{ij} \dot{\varepsilon}_{ij}, \qquad \dot{\varepsilon}_{ij} = \frac{1}{2}(\nabla_i v_j + \nabla_j v_i), \qquad \sigma_{ij} = -p\delta_{ij} + S_{ij}, \tag{1}$$

$$m_1 = \frac{4}{3}\pi a^3 n, \qquad i, j = 1, 2, 3,$$

where a and n are the pore radius and concentration, m_1 is the volume concentration of the pores (porosity), m_2 is the volume concentration of the material, ρ_s is the density of the material, ρ is the mean density, σ_{ij} and $\dot{\varepsilon}_{ij}$ are the averaged tensors of stress and strain rate, v_i is the ith component of velocity, E is the specific internal energy, p is the pressure, and S_{ij} is the deviator of the stress tensor.

Prior to compacting, the powder is assumed to be compressed to the state of dense packing; therefore, upon explosive loading, it behaves as a porous body with initial porosity $m_1^0 = 0{,}4$.

To close system (1), we used the equation of state of a porous body proposed in [6]

$$\dot{p} = \dot{p}_x + \dot{p}_t, \qquad \dot{p}_x = -K\dot{\varepsilon}^e_{kk}, \qquad \dot{p}_t = (\Gamma \rho E_t)',$$

$$E = E_x + E_t, \qquad E_x = ((1/2)K_1(\varepsilon^e_{kk})^2 + \mu_1 e^e_{ij} e^e_{ij})/\rho, \qquad e_{ij} = e^e_{ij} + e^p_{ij}, \tag{2}$$

where K_1 and μ_1 are the averaged elastic moduli of volume compression and shear of the porous material.

In the region of elastic deformations $(3/2)S_{ij}S_{ij} < Y^2$, the stress deviator is found from the Hooke's law

$$\overset{\nabla}{S}_{ij} = 2\mu \dot{e}_{ij}, \qquad \dot{e}_{ij} = \dot{\varepsilon}_{ij} - (1/3)\dot{\varepsilon}_{kk}\delta_{ij}, \tag{3}$$

and in the plastic region, from the Prandtl–Reiss equations

$$\dot{e}_{ij} = \overset{\nabla}{S}_{ij}/(2\mu) + \dot{\lambda} S_{ij}, \qquad (3/2)S_{ij}S_{ij} = Y^2,$$

$$\overset{\nabla}{S}_{ij} = \dot{S}_{ij} - \omega_{ik}S_{kj} - \omega_{jk}S_{ki}, \qquad \omega_{ij} = 0.5(v_{i,j} - v_{j,i}). \tag{4}$$

In (1)–(4), p_x and p_t are the "cold" and thermal pressures, E_x and E_t are the "cold" and thermal energies, K is the modulus of volume compression, μ is the shear modulus, Y is the yield strength, and Γ is the Grüneisen constant; each of the subscripts i, j, and k runs through the values of 1, 2, and 3; summation is performed

over repeated subscripts; the dot above a symbol corresponds to its derivative in time; the subscript after the comma refers to the derivative relative to the corresponding coordinate; elastic and plastic deformations are denoted by the subscripts e and p, respectively. The yield surface has the form

$$\frac{3}{2}S_{ij}S_{ij} = Y^2, \qquad Y^2 = \begin{cases} Y_s^2 m_2^2 - (9/4)p^2 m_1, & |p| \leqslant |p_0|, \\ Y_s^2 m_2 m_e^2, & |p_0| < |p| \leqslant |p_*|, \\ 0, & |p| > |p_*|, \end{cases} \tag{5}$$

$$m_e^2 = \frac{1+m_1^2}{m_2} - 2\frac{m_1}{m_2}\operatorname{ch}\frac{3p}{2Y_s}, \qquad m_e + m_p = 1,$$

where $|p_*| = (2/3)Y_s \ln(1/m_1)$; $|p_0| = (2/3)Y_s(1-m_1)$; Y_s is the yield strength of the continuous material, and m_e and m_p are the fractions of the cell volume, which are in the elastic and plastic states. It follows from formulas (5) that, as the pressure $|p|$ increases, the yield strength decreases and vanishes at $|p| = |p_*|$.

In the case $|p| < |p_0|$, elastic loading (unloading) occurs, and the following formulas are valid:

$$K = K_1, \quad \mu = \mu_1, \quad K_1 = K_s m_2 \Big/ \Big(1 + \frac{m_1}{2}\frac{1+\nu}{1-2\nu}\Big), \quad \mu_1 = \frac{\mu_s m_2}{1+0.5m_1}, \quad \dot{\varepsilon}_{kk}^e = -\frac{\dot{\rho}_s}{\rho_s}, \tag{6}$$

Here K_s and μ_s are the elasticity moduli of the continuous material and ν is the Poisson's ratio. In the case $|p_0| < |p| < |p_*|$, a plastic zone is formed around the pore, the strains become elastoplastic, and the following formulas are valid:

$$K = K_2, \qquad \mu = \mu_2, \qquad K_2 = K_s m_2 \Big/ \Big(1 + \frac{1+\nu}{3(1-2\nu)}\frac{Y}{|p|}m_p m_2\Big),$$

$$\mu_2 = \mu_s m_e \Big/ \Big(\frac{m_e}{m_2} + \frac{m_p}{2}\Big), \qquad e_{ij}^e = \frac{S_{ij}}{2\mu_1}, \qquad \dot{\varepsilon}_{kk}^e = \frac{K_2}{K_1}\dot{\varepsilon}_{kk}, \qquad \dot{\varepsilon}_{kk} = -\frac{\dot{\rho}}{\rho}. \tag{7}$$

Equations (7) are satisfied in the case of the loading $p\dot{p} > 0$. Upon unloading ($p\dot{p} < 0$), the material is described by Eqs. (6) to a certain state; the subsequent unloading from this state is elastic. If $|p| > |p_*|$, the pores lose their stability, and their collapse is observed. In this case, the equations acquire the form

$$\dot{p}_x = -K_1\dot{\varepsilon}_{kk}^e, \qquad \dot{\varepsilon}_{kk}^e = \dot{m}_2/m_2 - \dot{\rho}/\rho.$$

The variation of the quantity $\alpha(t, \alpha_0, p) = 1/m_2$ is described by the equation [6, 7]

$$p = \frac{\rho_s a_0^2}{3(\alpha_0 - 1)^{2/3}}\Big\{\ddot{\alpha}[\alpha^{-1/3} - (\alpha-1)^{-1/3}] + \frac{\dot{\alpha}^2}{6}[(\alpha-1)^{-4/3} - \alpha^{-4/3}]\Big\}$$

$$- \frac{4\eta\dot{\alpha}}{3\alpha(\alpha-1)} + \frac{2Y_s}{3}\ln\frac{\alpha}{\alpha-1}, \tag{8}$$

where η is the material viscosity.

In considering the pore-collapse dynamics behind the shock-wave front, we can distinguish two characteristic cases: inertial and viscous collapse of the pores. The ratio of inertial to viscous forces is determined by the Reynolds number analog $\mathrm{Re} = a_0\sqrt{Y_s\rho_s}/\eta$. Inertial forces prevail for $\mathrm{Re} \gg 1$, and viscous forces are dominant for $\mathrm{Re} \ll 1$. In the case $\mathrm{Re} \ll 1$, Eq. (8) takes the form

$$p = \frac{2}{3}Y_s \ln\frac{\alpha}{\alpha-1} - \frac{4}{3}\eta\frac{\dot{\alpha}}{\alpha(\alpha-1)}. \tag{9}$$

An estimate of the initial pore radius a_0 for which the inertial terms can be ignored yields the value of about 10 μm. Thus, for $a_0 \leqslant 10$ μm, the variation of porosity in time is described by Eq. (9), and in the case $a_0 > 10$ μm, it is necessary to solve the full equation (8).

Following Dunin and Surkov [7], we write the specific thermal energy E_t in the form

$$E_t = E_1 + E_2 + E_3, \qquad E_1 = \frac{2Y_s}{3\rho_s}\Big[\alpha_0 \ln\frac{\alpha_0}{\alpha} - (\alpha_0 - 1)\ln\frac{\alpha_0 - 1}{\alpha - 1} + (\alpha_0 - \alpha)\ln\frac{\alpha}{\alpha - 1}\Big],$$

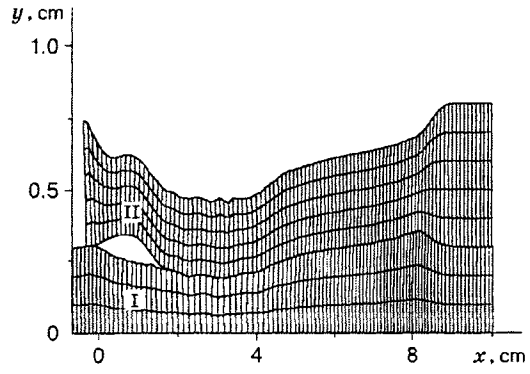

Fig. 2

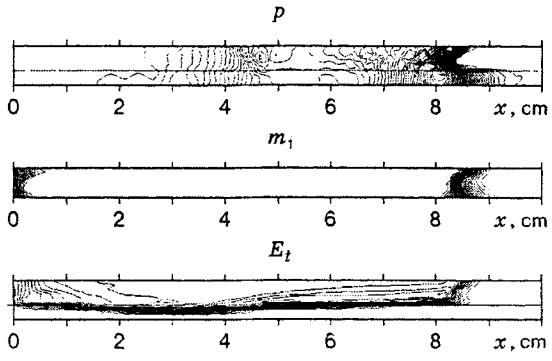

Fig. 3

$$E_2 = \frac{4\eta}{3\rho_s}\int \frac{\dot{\alpha}^2\,dt}{\alpha(\alpha-1)}, \qquad E_3 = \frac{a_0^2\dot{\alpha}^2}{6(\alpha_0-1)^{2/3}}\left[\frac{1}{(\alpha-1)^{1/3}} - \frac{1}{\alpha^{1/3}}\right],$$

where E_1 and E_2 are the mean values of dissipated energy in plastic and viscous flows and E_3 is the mean kinetic energy of motion arising upon collapsing of the pores.

The centerbody is an elastoplastic material, which is described by Eqs. (1) with $m_1 = 0$. As closing relations, we use Eqs. (2)–(4) in which we ignore the thermal energy $E_t = 0$ and, hence, the thermal pressure $p_t = 0$.

In this paper, the action of the explosion products on the powder was simulated by external pressure at the upper boundary of the powder. The value of this pressure was found from the analytical solution of the problem of motion of the explosion products behind the front of a one-dimensional plane detonation wave with an isentrope in the form $p = A\rho^\gamma$. In this case, all the parameters behind the shock-wave front depend only on the coordinate x and time t. The dependence of the velocity of sound $c(x,t)$ has the form [8]

$$c = x/(2t) + D/4 \quad \text{for} \quad D/2 < x/t < D,$$
$$c = D/2 \quad \text{for} \quad x/t < D/2.$$

Correspondingly, the pressure applied to the upper boundary of the powder at $\gamma = 3$ was found from the formula $p = p_H(c/c_H)^3$ (p_H and c_H are the pressure and velocity of sound at the Chapman–Jouguet point).

In the solution, we used the "cross" finite-difference scheme described in detail by Wilkins [9]. Nonphysical oscillations behind the shock-wave front were suppressed by introduction of artificial viscosity into the numerical scheme.

The contact boundaries are calculated using a symmetric algorithm developed by Gulidov and Shabalin [10].

The calculations were conducted for a plane case (Fig. 1). The plate material was aluminum, and the powder material was copper with initial porosity $m_1^0 = 0.38$. The detonation velocity varied within 0.2–0.8 cm/μsec. The volume velocity of sound in the aluminum plate was $C_0 = 0.535$ cm/μsec. The following parameters were used in the calculations: $\rho_s = 2.785$ g/cm^3, $Y_s = 0.41$ GPa, $K_s = 74.4$ GPa, and $\mu_s = 24.8$ GPa for aluminum and $\rho_s = 8.9$ g/cm^3, $Y_s = 0.2$ GPa, $K_s = 139$ GPa, and $\mu_s = 46$ GPa for copper.

Figures 2 and 3 show calculations results for the detonation velocity $D = 0.36$ cm/μsec ($D < C_0$) at the time $t = 25$ μsec. Figure 2 shows the difference grid in the plate (region I) and in the powder (region II). For convenience, the y scale is increased by a factor of seven. It is seen in Fig. 2 that a deformation hillock is formed on the surface of the aluminum plate for $D < C_0$; the influence of this hillock extends to the two nearest layers of the difference grid in the powder.

Figure 3 shows isolines of pressure p, porosity m_1, and specific thermal energy E_t. The horizontal solid line (for p and E_t) corresponds to the contact boundary powder–plate at the time $t = 0$. The isobars in Fig. 3 demonstrate the flow pattern formed in the computational domain. An incident shock wave in the powder and a weak shock wave emanating from the aluminum plate are clearly visible, and the propagation

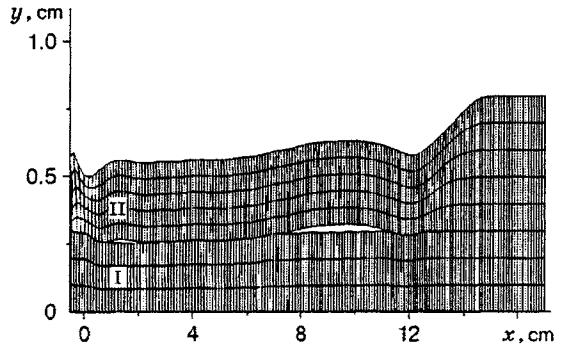

Fig. 4

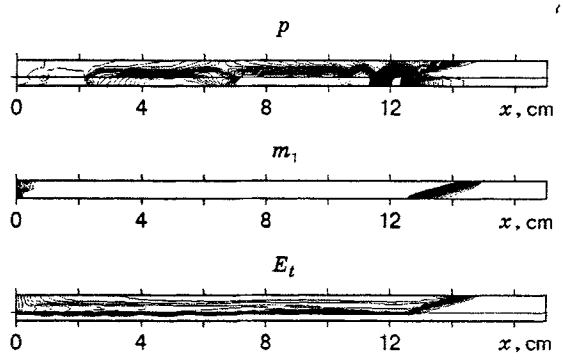

Fig. 5

of disturbances over the plate is observed. The distribution of porosity shows that a complete collapse of the pores occurs on the greater part of the sample. On the left, the powder was not compacted to the density of a continuous material because of the influence of an unloading wave passing from the butt-end surface. Far from the plate, the powder is compacted in an incident shock wave passing from the explosive. Near the interface between the powder and the plate, the pores collapse in a weak shock wave generated by the hillock, and this occurs earlier than the shock wave from the detonation products arrives. It is seen in Fig. 3 for E_t that this leads to a significant decrease in the thermal energy E_t in the powder near the plate. The thickness of the region of low thermal energy in the powder obtained in calculations varies within 0.18–0.27 cm, which extends to 2 or 3 cells of the computational grid. These values are in good agreement with experimental data [11]. The value of E_t decreases from 34 J/g to zero over this thickness. We note that the collapse of the pores and powder compacting near the plate prior to the arrival of the shock wave induced by the detonation products was observed in the experiments of Kostyukov [4].

Figures 4 and 5 show calculation results for the detonation velocity $D = 0.6$ cm/μsec, which is greater than the volume velocity of sound in the plate $C_0 = 0.535$ cm/μsec. The difference grid (Fig. 4) and the isolines of distributions of pressure p, porosity m_1, and specific thermal energy E_t (Fig. 5) are given for the time $t = 25$ μsec.

In this case, a deformation hillock is not observed on the plate surface (Fig. 4) (for convenience, the y scale is increased by a factor of ten). The reason is that the slope of the oblique shock wave in the powder is rather small. Thus, despite the fact that the compression wave in the plate goes ahead of the shock wave in the powder, the hillock on the interface between the powder and the plate does not have enough time to form before the arrival of the oblique shock wave. The isobars in Fig. 5 show that the powder compacting is uniform over the entire thickness in the incident shock wave emanating from the explosive. In this flow regime, the thermal energy E_t near the centerbody practically does not decrease [the dramatic decrease in E_t visible in Fig. 5 occurs over the thickness of the order of one cell of the computational grid; it is related to the use of linear interpolation utilized in constructing isolines from zero (in the plate) to the maximum].

The size of the deformation hillock depends on the difference in velocities $C_0 - D$. As the detonation velocity decreases, the hillock increases too, but this occurs up to a certain value of the detonation velocity. Thus, for $D = 0.2$ cm/μsec, the size of the hillock is smaller than for $D = 0.36$ cm/μsec. This dependence is explained by a smaller load on the powder during its compacting with lower velocities; hence, the action exerted by the plate decreases.

Thus, by means of numerical simulation of explosive compacting of powders in the two-dimensional formulation, it is shown that, the condition $D < C_0$ being satisfied, a deformation hillock is formed on the plate surface, which leads to the appearance of a "cold" layer.

REFERENCES

1. A. S. Kusubov, V. F. Nesterenko, M. L. Wilkins, et al., "Dynamic deformation of powdered materials as a function of particle size," in: *Proc. of the Int. Seminar on High Energy Working of Rapidly Solidified and High Temperature Superconducting Materials* (Novosibirsk, USSR, Oct. 10–14, 1988), Inst. Theor. and Appl. Mech., Sib. Div., Russian Acad. of Sci., Novosibirsk (1989), pp. 139–156.
2. N. A. Kostyukov, "Two-dimensional shock-wave flows and structure of powder compacts near the interface with a deformed target," *Model. Mekh.*, No. 6, 76–102 (1990).
3. S. P. Kiselev and V. M. Fomin, "Formation of a "cold" layer of particles upon explosive compacting of powders," *ibid.*, pp. 49–53.
4. N. A. Kostyukov, "Behavior of powder materials under conditions of two-dimensional shock-wave loading," Doctoral Dissertation in Phys.-Math. Sci., Novosibirsk (1993).
5. S. P. Kiselev and V. M. Fomin, "Model of a porous material considering the plastic zone near the pore," *Prikl. Mekh. Tekh. Fiz.*, **34**, No. 6, 125–133 (1993).
6. *Shock-Wave Processes in Two-Component and Two-Phase Media* [in Russian], Nauka, Novosibirsk (1992).
7. S. Z. Dunin and V. V. Surkov, "Effects of energy dissipation and melting on shock compression of porous bodies," *Prikl. Mekh. Tekh. Fiz.*, **23**, No. 1, 131–142 (1982).
8. K. P. Stanyukovich (ed.), *Physics of Explosion* [in Russian], Nauka, Moscow (1975).
9. M. L. Wilkins, "Calculation of elastoplastic flows," in: B. Alder, S. Fernbach, and M. Retenberg (eds.), *Methods of Computational Physics*, Vol. 3, Academic Press, New York (1964).
10. A. I. Gulidov and I. I. Shabalin, "Numerical implementation of boundary conditions in dynamic contact problems," Preprint No. 12, Inst. Theor. and Appl. Mech., Sib. Div., Russian Acad. of Sci., Novosibirsk (1987).
11. N. A. Kostyukov, "Physical causes and mechanisms of the formation of boundary regions in the two-dimensional explosive compaction of powdered materials," *Prikl. Mekh. Tekh. Fiz.*, **32**, No. 6, 154–161 (1991).